Quinoline-based tetrazolium prochelators: formazan release, iron sequestration, and antiproliferative efficacy in cancer cells

Yu-Shien Sung a and Elisa Tomat *a

Iron-binding strategies in anticancer drug design target the key role of iron in cancer growth. The incorporation of a quinoline moiety in the design of tetrazolium-based prochelators facilitates their intracellular reduction/activation to iron-binding formazans. The new prochelators are antiproliferative at submicromolar levels, induce apoptosis and cell cycle arrest, and impact iron signaling in cancer cells.

Iron is critical for maintaining the rapid proliferation rates that characterize cancer cells. This ubiquitous metal is also implicated in remodeling the tumor microenvironment, epithelial-mesenchymal plasticity and cancer cell stemness, as well as ferroptosis. The prominent role of iron in cancer biology is currently viewed as a targetable vulnerability in anticancer drug discovery. Several iron chelators (e.g., DFO, DFX, Triapine) have been tested or are currently under investigation in clinical trials, either alone or in combination with known chemotherapeutics. More recent iron-binding compounds, such as VLX6008, and ironomycin, are revealing new potential therapeutic avenues.

To avoid side effects associated with systemic metal binding, prochelators are being designed to release the active chelators only after cellular uptake.^{5, 11, 12} In addition, bioconjugation strategies, for instance to carbohydrates¹³ or serum albumin,¹⁴ have been pursued to facilitate accumulation in malignant cells relative to normal cells. Thiol-reactive¹⁵ and reductively activatable prochelators¹⁶⁻¹⁸ are generally advantageous because they capitalize on the higher glutathione (GSH) concentrations and more reducing cytoplasmic environment of malignant cells with respect to the surrounding tissue.¹⁹

Tetrazolium-based prochelators utilize the chemistry of the most common probe of cell viability, namely the intracellular reduction of the MTT cation (i.e., 3-(4,5-dimethyl-2-thiazolyl)-2,5-diphenyl-tetrazolium) to a formazan species that is detected colorimetrically.²⁰ We have shown that *N*-pyridyl tetrazolium prochelators (i.e., **2b**, **4b**, **Fig. 1a**) remain stable in blood serum but are reduced intracellularly to release the corresponding formazans.¹⁸

These metal-binding compounds in turn coordinate Fe(II) and disrupt intracellular iron homeostasis. The antiproliferative activities of these prochelators, however, are moderate, remaining in the 12–30 μM range in several cancer cell lines. In this work, we engineer a new generation of tetrazolium prochelators that exhibit antiproliferative activities at submicromolar concentrations.

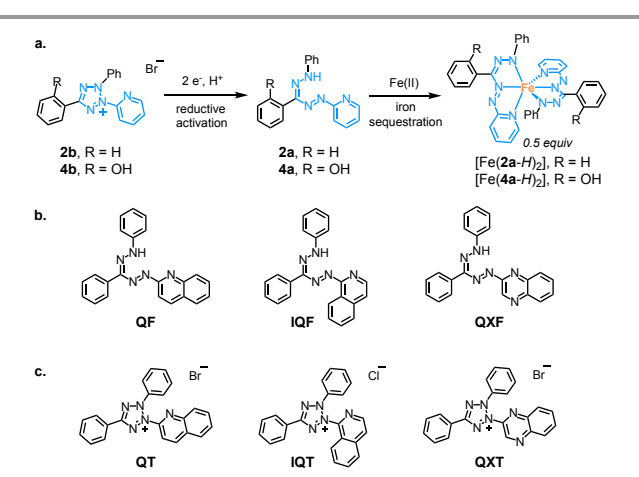


Figure 1. Prochelation strategy (a) based on the intracellular reduction of *N*-pyridyl tetrazolium cations to liberate iron-binding formazan ligands. Formazan (b) and tetrazolium (c) compounds investigated in this study featuring quinolyl, isoquinolyl, and quinoxalyl donor groups.

The two-electron reduction of tetrazolium prochelators in the intracellular environment is crucial to their activation through the formation of antiproliferative formazan chelators. The activation of $\bf 2b$ and $\bf 4b$ was found to be incomplete after 48-hour incubations and likely limited their efficacy. We reasoned that a more rapid and effective reduction would lead to a larger fraction of released chelators and thus to enhanced iron sequestration. As such, we sought to incorporate quinoline, isoquinoline, or quinoxaline into the new constructs with the intent to (i) maintain the same coordination mode of the pyridyl systems, and (ii) shift anodically the new reduction potentials due to the more electron-withdrawing, π -extended heterocycles.

The target formazan compounds (QF, IQF, and QXF, Fig. 1b) were obtained by reacting benzene diazonium chloride with the appropriate hydrazone in basic conditions in a

^a-Department of Chemistry and Biochemistry, The University of Arizona, Tucson, AZ 85721-0041, United States

Electronic Supplementary Information (ESI) available: Synthetic procedures and characterization data, details of crystallographic analysis, experimental protocols for in vitro tests and biological assays in cultured cells. See DOI: 10.1039/x0xx00000x

water/dimethylformamide mixture (**Scheme S1**). All three compounds coordinate Fe(II) in aqueous mixtures (50 mM HEPES and DMSO, 7:3 v/v, pH 7.4). The formazan solutions exhibited a color change from red/pink to purple upon Fe(II) addition, with **QF** and **IQF** presenting a significant increase in absorbance beyond ~600 nm (**Figs. 2a, S2**). HPLC-LRMS analysis confirmed the formation of iron complexes with a 2:1 ligand-to-metal stoichiometry (**Fig. S3**).

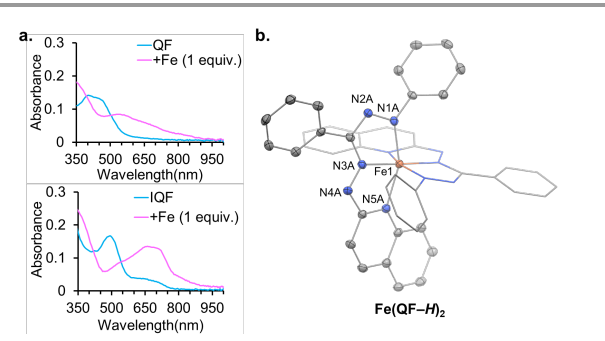


Figure 2. (a) Optical absorbance changes of **QF** and **IQF** after addition of ferrous ammonium sulfate in 50 mM HEPES buffer and DMSO (7:3, v/v) at pH 7.4. (b) Crystal structure of Fe(**QF**-H)₂ showing a partial atom labeling scheme. Thermal ellipsoids are scaled to the 50% probability level. One of the ligands is shown as wireframe and hydrogen atoms are omitted for clarity (CCDC 2336932).

The iron coordination geometry of formazan \mathbf{QF} was investigated by X-ray crystallography (Fig. 2b, Tables S1-S2). The complex was obtained by adding $Fe(BF_4)_2 \cdot 6H_2O$ (1.0 equiv.) to \mathbf{QF} in ethanol at room temperature. Single-crystal diffraction analysis revealed a distorted octahedral complex with two monoanionic tridentate ligands. Consistent with the reported N-pyridyl formazan iron complexes, 18 the two ligands bind in the same way through nitrogen atoms N1A and N3A on the formazan moiety and the quinoline nitrogen N5A. Complex $Fe(\mathbf{QF}-H)_2$ is neutral and the NMR characterization data are indicative of a diamagnetic species, thus assigning a low-spin electronic configuration to the Fe(II) center.

The tetrazolium compounds **QT** and **QXT** (**Fig. 1c**) were synthesized through the oxidation of the corresponding formazans using *N*-bromosuccinimide (NBS) in ethyl acetate (**Scheme S2**). Because some unintended bromination was observed in the case of the isoquinoline analog in the presence of NBS, **IQT** (**Fig. 1c**) was synthesized using Pb(OAc)₄ as an oxidant (**Scheme S2**).

As expected in this prochelation design, the positively charged tetrazolium compounds do not coordinate metal ions in solution, and no changes were observed in their optical absorption spectra upon addition of Fe(II) in buffered aqueous media (**Fig. S5**). Their distribution coefficients ($log D_{o/pH7.4}$) range between 0.4 and 1.0 (**Table S3**), thus indicating that all three compounds are rather amphiphilic and well distributed between octanol and phosphate-buffered saline solution (PBS, pH 7.4).

To assess the reduction/activation of the new tetrazolium prochelators, reduction potentials (E_{red}) were recorded by cyclic voltammetry in aqueous solutions (PBS, pH 7.4) using potassium ferricyanide (K_3 FeCN₆, E_0 0.430 V vs NHE)²¹ as a reference (**Fig. S6**). Consistent with the known reduction mechanism involving

the generation of a tetrazolinyl radical, subsequent formation of the formazan anion, and protonation, 22 the tetrazolium compounds present an irreversible two-electron reduction. The reduction potentials (E_{red}) vary based on the electronic effects of heterocyclic substituents on the tetrazolium core. **QT** displays two relatively broad one-electron events with the first reduction at -22 mV, and **IQT** has two overlapping events at -52 mV. (**Fig. S6**) The additional electron-withdrawing nitrogen atom in the heterocycle of **QXT** shifted the E_{red} anodically to 59 mV. Whereas the previous tetrazolium prochelators **2b** and **4b** had E_{red} values below -100 eV, 18 the compounds in the new series are significantly easier to reduce.

Critically, the chemical reduction of the new tetrazolium compounds was observed in the presence of common bioreductants sodium ascorbate and glutathione (GSH). **QT**, **IQT** and **QXT** (100 μ M) were reduced faster than **2b** and **4b** by ascorbate (5 mM) in a phosphate buffer mixture (pH 7.4, 30% DMSO). Over 80% conversions were achieved within 20 min, compared to ~80 min for **2b** and **4b** (**Fig. 3a**). The solutions changed from colorless to red/orange upon formation of the formazan products. The reduction kinetics followed the same trend in the presence of GSH (5 mM, **Fig. 3b**), a key intracellular reductant found at millimolar concentrations in the cytosol. ¹⁹ The *N*-quinoxalyl analog was reduced faster than the *N*-quinolyl ones, which were in turn more reactive than the *N*-pyridyl systems. We observed that >50% of **QT** and **IQT** were reduced by GSH to formazans within 3 hours.

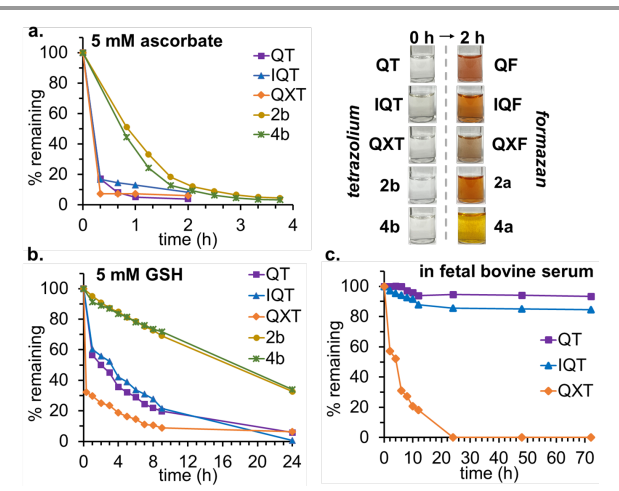


Figure 3. Reduction kinetics of tetrazolium cations (100 μ M) as monitored by HPLC at pH 7.4 (100 mM phosphate buffer/DMSO, 7:3 ν/ν) and 37 °C in the presence of (a) sodium ascorbate (5 mM) and (b) glutathione (5 mM). Representative photos of the solutions before and after reduction by ascorbate are shown in panel (a). The stability of the new tetrazolium compounds (1.0 mM) was also tested in fetal bovine serum (c).

Prior to testing the prochelators in cultured cells, we assessed their stability in fetal bovine serum (FBS) by HPLC analysis. **QT** and **IQT** are essentially stable in FBS for 72 hours (**Fig. 3c**). In contrast, **QXT** was readily reduced by the bioreductants present in FBS and completely converted to formazan within 4 hours (**Figs. 3c, S7**). **QXT** is therefore similar to the MTT dye, which has a similar reduction potential¹⁸ and is known to be prone to reduction in FBS.²³

Journal Name COMMUNICATION

The antiproliferative activity of the tetrazolium compounds was tested in metastatic breast cancer cells (MDA-MB-231) and in ovarian cancer cells (A2780) because the role of iron is well-established in these cancer types. $^{24, 25}$ Normal lung fibroblasts (MRC-5) were included for comparison to a non-malignant cell line. The IC50 values were measured after 72-hour incubations using the fluorescent-based resazurin assay (**Table 1**).

Chelator deferasirox (DFX) served as a control compound known for its antiproliferative activity attributed to iron deprivation. Consistent with its reported toxicities in mammalian cells, ²⁶ the IC₅₀ values for DFX were in the moderate micromolar range (10–20 μ M) in the tested cancer cell lines and $^{\sim}180~\mu M$ in the normal cells, which typically exhibit lower sensitivity to iron deprivation. Notably, prochelators QT and IQT displayed antiproliferative activities in the submicromolar range $(0.3-0.8 \mu M)$ in cancer cells and low micromolar levels in normal cells (6–10 μM). In contrast, the corresponding formazan chelators QF and IQF present lower activities in all cell lines. These findings highlight the advantages of the prochelation strategy: when compared to the lipophilic formazan chelators, the amphiphilic, water-soluble tetrazolium cations likely present superior cellular uptake and also protect the metalbinding unit from unwanted reactivity in the extracellular milieu. Consistently, QXT, which was found to be readily reduced in serum (Fig. 3c), lacked the prochelation advantage and exhibited antiproliferative activities similar to those of the corresponding formazan QXF in malignant and normal cells.

Table 1. Comparison of antiproliferative activities in cultured cells

Compound	IC ₅₀ (μΜ, 72 h)		
	MDA-MB-231	A2780	MRC-5
DFX	15 ± 2	12 ± 2	180 ± 30
QT	0.3 ± 0.1	0.8 ± 0.1	6.2 ± 0.5
QF	7 ± 2	14 ± 2	90 ± 9
IQT	0.6 ± 0.1	0.5 ± 0.1	10 ± 2
IQF	3.2 ± 0.5	4.8 ± 0.1	21 ± 3
QXT	26 ± 3	19 ± 2	45 ± 8
QXF	22 ± 3	9 ± 2	11 ± 2

 IC_{50} values (μ M) obtained using the resazurin assay after exposure to test compounds (0.032–100 μ M or 0.8–500 μ M) for 72 h (mean ± SDM, n=3).

The submicromolar antiproliferative activities of the new prochelators \mathbf{QT} and \mathbf{IQT} are significantly improved with respect to those of the reported N-pyridyl tetrazolium compounds $\mathbf{2b}$ and $\mathbf{4b}$, which had IC₅₀ values in the moderate micromolar range (12–17 μ M in the tested breast and ovarian carcinoma cells). ¹⁸ This difference is likely attributable to better activation of the new tetrazolium cations, which have higher reduction potentials and faster reduction kinetics (*vide supra*) resulting in a larger fraction of activated formazan chelators. To further characterize the intracellular activation and biological activities of \mathbf{QT} and \mathbf{IQT} , we assessed their effects on cell cycle, cell death, and intracellular iron sequestration in A2780 cells.

Because iron is critical for cell proliferation, iron sequestration typically induces cell cycle arrest in the G_1 or S phases and activates apoptotic pathways. Based on DNA content levels measured by flow cytometry, our cell cycle analysis after 24-hour incubations indicated that chelator control DFX (50 μ M) and prochelator QT (5 μ M) caused cell accumulation in the S-phase whereas IQT (5 μ M) led to G1 arrest (Figs. 4a, S8). At the same concentrations, cell death assay by flow cytometry showed that all three compounds induce apoptosis after 48 hours, with the combined percentage of cells stained by AnnexinV in early and late apoptosis ranging from 17% to 20% (Figs. 4b, S9). Indeed QT and IQT are significantly more potent than 2b and 4b, causing similar apoptotic effects at a micromolar dose lower by approximately one order of magnitude (i.e., 5.0 vs 40 μ M).

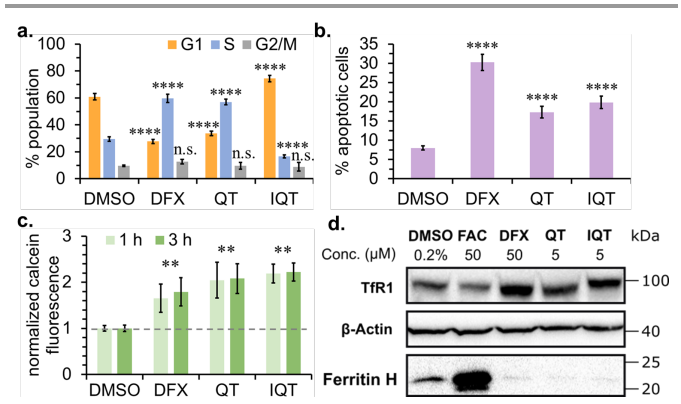


Figure 4. Effects of DFX (50 μ M), **QT** and **IQT** (5 μ M) on A2780 cancer cells. (a) Cell cycle assay. (b) Apoptosis assay using Annexin V-FITC as a probe, combining the cells in early and late apoptosis. (c) Assessment of intracellular iron binding through calcein assays. (d) Representative gel images of Western blot, transferrin receptor 1 (TfR1), and ferritin heavy chain (ferritin H). FAC, ferric ammonium citrate. All *t*-tests relative to vehicle only (DMSO): **p < 0.01, ****p < 0.0001, n.s. not significant.

Next, we investigated the ability of the new prochelators to disrupt intracellular iron availability. In the calcein assay, the fluorescence of the probe is initially quenched by intracellular, paramagnetic iron ions and then restored by effective iron scavengers. A2780 cells were first treated with the cell-permeant calcein-AM probe (0.1 μ M) for 30 min and subsequently incubated with the test compounds for 1 and 3 hours. We observed a rapid restoration of calcein fluorescence in all cases: in fact both QT and IQT caused higher fluorescence increases compared to the control DFX (Fig. 4c). The fluorescence changes appear to saturate within one hour, suggesting a rapid cellular uptake and activation of the cationic prochelators.

We further validated the intracellular formation of iron complexes by uHPLC-HRMS analysis of the cell lysates after 48-hour incubations with the prochelators **QT** and **IQT**. Semi-quantitative analysis of the chromatography and mass spectrometry data (**Fig. S10**) indicate that **QT** and **IQT** are mostly found as reduced formazans, and a small iron-bound fraction (with a 2:1 ligand-to-metal stoichiometry) is detected in both cases. Collectively, the calcein assays on intact cells and the analysis of cell lysates confirm that the tetrazolium prochelators

undergo cellular uptake and intracellular reduction to generate formazan chelators that bind intracellular labile iron.

We also assessed the ability prochelators QT and IQT to impact intracellular iron signaling. Specifically, we investigated by Western blot analysis the expression levels of transferrin receptor 1 (TfR1), which is key to iron uptake, and ferritin heavy chain (ferritin H), a subunit of the major iron storage protein ferritin. The expression levels of these iron handlers are carefully controlled by iron regulatory proteins (IRPs) and serve as sensitive markers of the cellular iron status. As expected in response to iron deficiency, cells treated with control DFX (50 μ M) and with QT and IQT (5 μ M) present upregulation of TfR1 and degradation of ferritin (Figs. 4d, S11). In contrast, iron supplementation with ferric ammonium citrate (FAC, 50 μM) caused decreased TfR1 expression and upregulation of ferritin, indicating that cells experience iron repletion (Figs. 4d, S11). Notably, the effects of prochelators **QT** and **IQT** were evident at a 10-fold lower concentration relative to DFX, consistent with the higher toxicity of the tetrazolium compounds and indicative of their prompt activation in cells.

Finally, we confirmed the role of iron in the cytotoxicity of **QT** and **IQT** by reassessing the IC₅₀ values in full growth media supplemented with FAC (50 μ M). In both cases, the 72-hour IC₅₀ values increased significantly from submicromolar concentrations to approximately 3 μ M (**Fig. S12**).

In conclusion, we have shown that the introduction of a quinoline moiety substantially increases the potency of antiproliferative tetrazolium prochelators. When compared to the pyridine-based systems, the new QT and IQT prochelators are reduced more rapidly and efficiently by biological reductants (e.g., ascorbate, glutathione) but remain stable in blood serum. Their intracellular reduction releases chelators that bind Fe(II) through two formazan nitrogen atoms and a quinoline donor. Critically, these quinoline-based tetrazolium compounds with optimal reduction potentials exhibited submicromolar IC50 values in breast and ovarian cancer cells, whereas cytotoxicity levels were significantly lower in normal fibroblasts. We demonstrated that the antiproliferative activity of QT and IQT is associated to cell cycle arrest, apoptosis, and intracellular iron deprivation. Overall, this work showcases the engineering of the tetrazolium prochelator core to achieve improved antiproliferative activity for applications in anticancer

This work was funded by the US National Institutes of Health (R35 GM153364). We thank Iva Habensus for assistance with X-ray data acquisition and analysis. The diffractometer in our Department of Chemistry and Biochemistry was acquired thanks to the National Science Foundation (CHE-2117516). The UArizona Cancer Center Flow Cytometry Shared Resource is supported by the National Cancer Institute (P30 CA023074).

Conflicts of interest

There are no conflicts to declare.

Notes and references

- L. S. V. Torti and F. M. Torti, *Cancer Res.*, 2020, **80**, 5435-5448.
- 2. A. DeRosa and A. Leftin, Front. Immunol., 2021, 12, 614294.
- R. Rodriguez, S. L. Schreiber and M. Conrad, *Mol. Cell*, 2022, 82, 728-740.
- G. Lei, L. Zhuang and B. Gan, Nat. Rev. Cancer, 2022, 22, 381-396.
- 5. E. Tomat, Curr. Opin. Chem. Biol., 2023, **74**, 102315.
- G. Y. Lui, Z. Kovacevic, V. Richardson, A. M. Merlot, D. S. Kalinowski and D. R. Richardson, *Oncotarget*, 2015, 6, 18748-18779.
- 7. P. Heffeter, V. F. S. Pape, É. A. Enyedy, B. K. Keppler, G. Szakacs and C. R. Kowol, *Antioxid. Redox Signal.*, 2019, **30**, 1062-1082.
- L. Reisbeck, B. Linder, G. Tascher, S. Bozkurt, K. J. Weber, C. Herold-Mende, S. J. L. v. Wijk, R. Marschalek, L. Schaefer, C. Münch and D. Kögel, Am. J. Physiol. Cell Physiol., 2023, 325, C1451-C1469.
- 9. V. Pósa, A. Federa, K. Cseh, D. Wenisch, G. Spengler, N. V. May, N. Lihi, G. F. Samu, M. A. Jakupec, B. K. Keppler, C. R. Kowol and É. A. Enyedy, *Inorg. Chem.*, 2024, **63**, 2401-2417.
- J. Devin, T. Cañeque, Y.-L. Lin, L. Mondoulet, J.-L. Veyrune, M. Abouladze, E. Garcia De Paco, O. Karmous Gadacha, G. Cartron, P. Pasero, C. Bret, R. Rodriguez and J. Moreaux, Cancer Res., 2022, 82, 998-1012.
- 11. Q. Wang and K. J. Franz, Acc. Chem. Res., 2016, 49, 2468-2477.
- A. Steinbrueck, A. C. Sedgwick, J. T. Brewster, K.-C. Yan, Y. Shang, D. M. Knoll, G. I. Vargas-Zúñiga, X.-P. He, H. Tian and J. L. Sessler, *Chem. Soc. Rev.*, 2020, 49, 3726-3747.
- Y.-S. Sung, B. Kerimoglu, A. Ooi and E. Tomat, ACS Med. Chem. Lett., 2022, 13, 1452-1458.
- 14. Y.-S. Sung, W. Wu, M. A. Ewbank, R. D. Utterback, M. T. Marty and E. Tomat, *ChemMedChem*, 2021, **16**, 2764-2768.
- W. Wu, Y.-S. Sung and E. Tomat, *Inorg. Chem.*, 2022, 61, 19974-19982.
- C. Mertens, E. A. Akam, C. Rehwald, B. Brüne, E. Tomat and M. Jung, *PLOS ONE*, 2016, 11, e0166164.
- E. A. Akam, R. D. Utterback, J. R. Marcero, H. A. Dailey and E. Tomat, *J. Inorg. Biochem.*, 2018, **180**, 186-193.
- Z. Xu, Y.-S. Sung and E. Tomat, J. Am. Chem. Soc., 2023, 145, 15197-15206.
- L. Kennedy, J. K. Sandhu, M. E. Harper and M. Cuperlovic-Culf, Biomolecules, 2020, 10, 1429.
- J. C. Stockert, R. W. Horobin, L. L. Colombo and A. Blázquez-Castro, Acta Histochem., 2018, 120, 159-167.
- 21. P. Leslie Dutton, in *Methods in Enzymology*, Academic Press, 1978, vol. 54, pp. 411-435.
- 22. U. Kisaburo, Bull. Chem. Soc. Jpn., 1989, 62, 3783-3789.
- D. Funk, H.-H. Schrenk and E. Frei, *BioTechniques*, 2007, 43, 178-186.
- D. Basuli, L. Tesfay, Z. Deng, B. Paul, Y. Yamamoto, G. Ning, W. Xian, F. McKeon, M. Lynch, C. P. Crum, P. Hegde, M. Brewer, X. Wang, L. D. Miller, N. Dyment, F. M. Torti and S. V. Torti, Oncogene, 2017, 36, 4089-4099.
- Z. K. Pinnix, L. D. Miller, W. Wang, R. D'Agostino, T. Kute, M. C. Willingham, H. Hatcher, L. Tesfay, G. Sui, X. Di, S. V. Torti and F. M. Torti, Sci. Transl. Med., 2010, 2, 43ra56.
- G. Y. L. Lui, P. Obeidy, S. J. Ford, C. Tselepis, D. M. Sharp, P. J. Jansson, D. S. Kalinowski, Z. Kovacevic, D. B. Lovejoy and D. R. Richardson, *Mol. Pharmacol.*, 2013, 83, 179.
- 27. N. T. V. Le and D. R. Richardson, *Biochim. Biophys. Acta, Rev. Cancer*, 2002, **1603**, 31-46.
- W. Breuer, S. Epsztejn and Z. I. Cabantchik, J. Biol. Chem., 1995, 270, 24209-24215.